

New results for $K^+ \rightarrow \pi^+ \nu \bar{\nu}$ at low π^+ momentum from BNL E949

A. Shaykhiev (for E949 Collaboration)

Abstract The BNL E949 experiment was a successor to BNL E787 and was aimed to measure the branching ratio of the $K^+ \rightarrow \pi^+ \nu \bar{\nu}$ decay. After detector upgrades were made, data equivalent to 1.7×10^{12} K^+ decays at rest were collected in a 2002 physics run. The data were analyzed via a blind analysis with a technique called the "Bifurcation Method". In this report we present the results of a search for $K^+ \rightarrow \pi^+ \nu \bar{\nu}$ in the pion momentum region below $K^+ \rightarrow \pi^+ \pi^0$ peak. Three new candidate events were observed with an estimated background of $0.93 \pm 0.17^{+0.32}_{-0.24}$ events. Combining these observation with previously reported results yields a branching ratio of $BR(K^+ \rightarrow \pi^+ \nu \bar{\nu}) = (1.73^{+1.15}_{-1.05}) \times 10^{-10}$ consistent with the standard model prediction.

1 Introduction

The Standard Model (SM) in particle physics has accounted for almost all particles and their processes have observed.

CP violation was discovered in the middle of the 1960's and reasonable explanations for the mechanism of CP violation have been explored for years. Kobayashi and Maskawa explained CP violation by introducing 3×3 unitary matrix with imaginary phase. The unitary matrix has four independent parameters, which in the Wolfenstein parameterization are A , λ , ρ and η . In terms of these parameters, the Cabbibo-Kobayashi-Maskawa (CKM) matrix can be written as

$$\begin{pmatrix} V_{ud} & V_{us} & V_{ub} \\ V_{cd} & V_{cs} & V_{cb} \\ V_{td} & V_{ts} & V_{tb} \end{pmatrix} \simeq \begin{pmatrix} 1 - \lambda^2/2 & \lambda & A\lambda^3(\rho - i\eta) \\ -\lambda & 1 - \lambda^2/2 & A\lambda^2 \\ A\lambda^3(1 - \rho - i\eta) & -A\lambda^2 & 1 \end{pmatrix} \quad (1)$$

A. Shaykhiev
Institute for Nuclear Research RAS, 60 October Revolution Pr. 7a, 117312 Moscow, Russia, e-mail: shaykhiev@inr.ru

CP invariance of the Lagrangian for weak interaction is violated when the CKM matrix is a complex one. The parameter η describes CP violation in the SM. One of the most important goals of experimental physics is to determine the CKM matrix elements.

All of direct and indirect information concerning the CKM matrix elements can be summarized in terms of "unitary triangles". Applying the unitary property $V^\dagger V = 1$ to the CKM matrix in (1) implies

$$V_{ub}^* V_{ud} + V_{cb}^* V_{cd} + V_{tb}^* V_{td} \simeq V_{ub}^* - \lambda V_{cb}^* + V_{td} = 0, \quad (2)$$

where the approximations $V_{ud} \simeq V_{tb}^* \simeq 1$ and $V_{cd} \simeq -\lambda$ have been made. This equation is represented graphically in Figure 1.

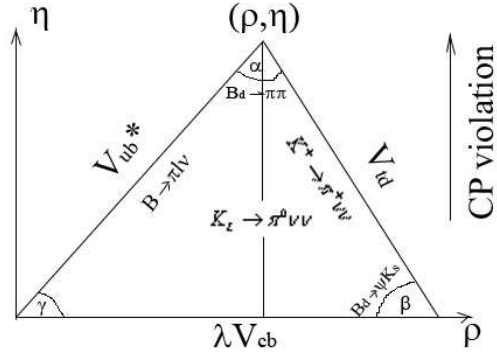


Fig. 1 Unitary triangle in the ρ - η plane

Powerful tests of our understanding of CP violation and quark mixing will come from comparisons of the results from B meson and kaon decays:

- A comparison of angle β from the ratio $BR(K_L^0 \rightarrow \pi^0 \nu \bar{\nu})/BR(K^+ \rightarrow \pi^+ \nu \bar{\nu})$ and from CP violation asymmetry in the decay $B_d^0 \rightarrow J/\psi K_s^0$.
- A better determination of $|V_{td}|$ from $K^+ \rightarrow \pi^+ \nu \bar{\nu}$ and from the mixing frequencies of B_s and B_d mesons will provide sensitive test of the SM and probe new physics.

1.1 Physics beyond the SM

Among the many rare kaon and B meson decays, the $K \rightarrow \pi \nu \bar{\nu}$ modes are unique since their SM branching ratios can be computed to an exceptionally high degree of precision, not matched by any flavour-changing neutral current process involving quarks. A possible discrepancy between the measured branching ratio and the SM

prediction would indicate the existence of new physics beyond the SM. For the $K^+ \rightarrow \pi^+ \nu \bar{\nu}$ decay SM branching ratio is $(0.85 \pm 0.07) \times 10^{-10}$ [7].

Several SM extensions to new physics would affect the $K^+ \rightarrow \pi^+ \nu \bar{\nu}$ branching ratio. For example, in the "Minimal Flavor Violation" model, where the origin of CP violation and quark mixing comes from the CKM matrix, as in the SM, the $K^+ \rightarrow \pi^+ \nu \bar{\nu}$ branching ratio is allowed to be as large as 1.9×10^{-10} [8].

1.2 Previous results of the search for $K^+ \rightarrow \pi^+ \nu \bar{\nu}$

A detailed history of the search for $K^+ \rightarrow \pi^+ \nu \bar{\nu}$ can be found in [3]. The first attempt to measure this decay was a heavy liquid bubble chamber experiment [9] at the Argonne Zero Gradient Synchrotron. The result of this experiment was a 90% CL upper limit on the branching ratio of 5.7×10^{-5} . About a decade later an experiment at KEK Proton Synchrotron improved the limit to 1.4×10^{-7} [6]. Previous results for BNL E787/E949 are summarized in Table 1.

Table 1 Previous results of the search for $K^+ \rightarrow \pi^+ \nu \bar{\nu}$

π^+ momentum (MeV/c)	(211,229)	(140,199)
Years	1995-98(E787) and 2002(E949)	1996-97(E787)
Stopped K^+	7.7×10^{12}	1.7×10^{12}
Candidates	3	1
$\text{BR}(K^+ \rightarrow \pi^+ \nu \bar{\nu})$	$(1.47^{+1.30}_{-0.89}) \times 10^{-10}$ (68% CL)	$< 22 \times 10^{-10}$ (90% CL)

2 Experiment BNL E949

The experimental signature of the $K^+ \rightarrow \pi^+ \nu \bar{\nu}$ decay is a single pion track and no other particle from a K^+ decay, because two neutrinos in the final state cannot be detected in the apparatus. $K^+ \rightarrow \pi^+ \nu \bar{\nu}$ is a three-body decay and the pion has the momentum $P_\pi < 227$ MeV/c.

2.1 The E949 detector

The K^+ beam is produced by a high-intensity proton beam from the Alternating Gradient Synchrotron (AGS) at Brookhaven National Laboratory (BNL). Protons are accelerated to a momentum of 21.5 GeV/c and hit the platinum target.

Incoming ~ 710 MeV/c kaons with $3/1 K^+/\pi^+$ ratio are identified by Čerenkov counter and two proportional wire chambers then slowed down by an inactive degrader and an active degrader (AD), passing through a beam hodoscope and stopping in the scintillating fiber target as shown schematically in Figure 2.

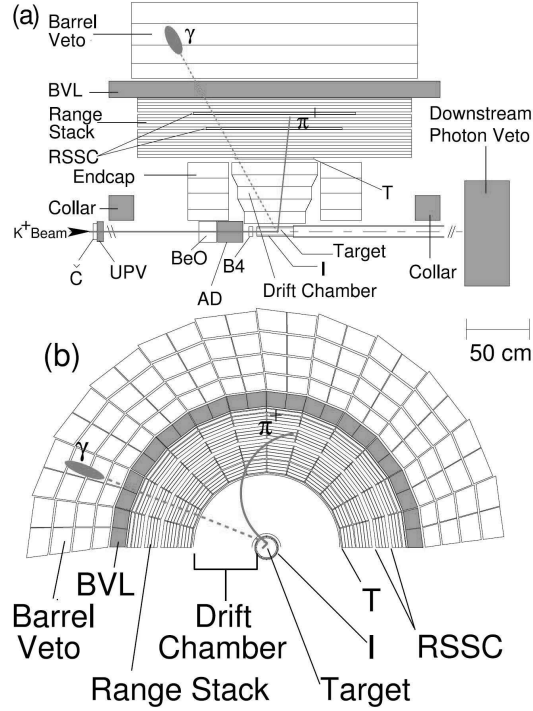


Fig. 2 Schematic side (a) and end (b) views of the upper half of the E949 detector. An incoming kaon is shown traversing the beam instrumentation stopping in the target and decaying to $\pi^+ \pi^0$. The outgoing charged pion and one photon from $\pi^0 \rightarrow \gamma\gamma$ decay are illustrated. Elements of the detector are described in the text.

The Čerenkov light from kaons and pions is unreflected and reflected at the inner surface of the radiator, respectively. The light from a kaon exits the radiator and is reflected by a parabolic mirror to the outer ring of 14 photomultiplier (PMT) tubes, while that from pion is internally reflected within the radiator and detected in the inner ring of 14 PMTs. Behind the Čerenkov counter, two beam wire chambers (BWPCs) are located. BWPCs allow to monitor beam profile and to identify multiple incoming particles. Downstream of BWPCs cylindrical degraders are located for slowing down the kaons so that come to rest in the center of the target. The inactive degrader is made of 11.1 cm long BeO and 4.76 mm Lucite. The AD consists of 40 layers of 2 mm thick scintillator disks (139 mm diameter) alternating with 2 mm thick copper disks (136 mm diameter). The AD is split into 12 azimuthal segments. The scintillation lights in the each segment are sent to a single PMT through wavelength shifting fibers and read out by ADCs, TDCs and CCDs. Using this information the AD allows to identify the beam particles and to detect the activities coincident with kaon decays. After passing through the degraders, just in front of

the target, a beam hodoscope (B4) detects the incoming particle and identifies it as a kaon by measuring the energy deposit.

The target consists of 413 5 mm square and 3.1 m long plastic scintillating fiber that are bundled to form 12 cm diameter cylinder. A number of smaller fibers ("edge" fibers) fill in the gaps near the outer edge of the target. Each 5 mm fibers is connected to a PMT, whereas the edge fibers are grouped into 12 and each group of the edge fibers is connected to a single PMT. The PMTs are read out by ADCs, TDCs and CCDs. The fiducial region of the target is defined by two layers of 6 plastic-scintillating counters that surround the target. The inner counters (IC) tag decay products for a trigger before they enter the drift chamber. The outer counters (VC) overlap the downstream edge of the IC by 6 mm and serve to detect particles that decay downstream of the fiducial region.

The drift chamber, called "Ultra Thin Chamber" (UTC), is located just outside of the IC. The whole E949 spectrometer is in a 1 Tesla magnetic field. Positively charged particles are bent clockwise in view from downstream. The primary functions of UTC are momentum measurement of charged particles and to provide a matching between the tracks in the target and in the range stack. The UTC consists of 3 superlayers. Each superlayer contains four layers of axial anode wires that provide xy position information between two cathode foil strips that provide z position information. The UTC has a length of 51 cm and inner and outer radii of 7.85 cm and 43.31 cm, respectively.

The range stack (RS) is located just outside the UTC at an inner radius of 45.08 cm and an outer radius of 84.67 cm. It consists of 19 layers of plastic scintillators azimuthally segmented into 24 sectors (Figure 2). The scintillators of layers 2–18 have a thickness of 1.905 cm and a length of 182 cm. The scintillators of 19 layer have a thickness of 1 cm and are mainly used to veto charged particles with long range by requiring that they do not reach the 19 layer. The innermost counters, called T-counters, serve to define the fiducial volume for kaon decay products. The scintillation light is led by light guides to PMTs. Each PMT of RS counters is read out by an ADC and a TDC. The primary functions of the RS are energy and range measurements of charged particles and their identification.

The detection of any activities coincident with the charged track is very important for suppressing the backgrounds for $K^+ \rightarrow \pi^+ \nu \bar{\nu}$ decay. Photons from $K_{\pi 2}$ and other radiative decays are detected by hermetic photons detectors with 4π solid angle coverage. Photon veto is performed by the Barrel Veto (BV), the Barrel Veto Linear (BVL), the upstream and downstream End Caps (ECs), the upstream and downstream Collar detectors (CO), the downstream Microcollar detector (MC), as well as the target and RS. The BV and BVL with a thickness of 14.3 and 2.29 radiation lengths (r.l.) at normal incidence, respectively, provide photon detection over $2/3$ of 4π solid angle. The photon detection over the remaining $1/3$ of 4π solid angle is provided by the other calorimeters in the region from $\approx 10^\circ$ to 45° of the beam axis with a total thickness from 7 to 15 r.l.

More detail description of the E949 experiment may be found in [3].

3 Data analysis

Identification of $K^+ \rightarrow \pi^+ \nu \bar{\nu}$ decays relies on detection of an incoming kaon, its decay at rest and an outgoing pion with no coincident detector activity. All other kaon decay modes could be sources of background. There are two kinematic regions to search for $K^+ \rightarrow \pi^+ \nu \bar{\nu}$ called $\pi \nu \bar{\nu}(1)$ and $\pi \nu \bar{\nu}(2)$ that lie above and below $K^+ \rightarrow \pi^+ \pi^0$ ($K_{\pi 2}$) peak, respectively (Figure 3). The $\pi \nu \bar{\nu}(1)$ region is more

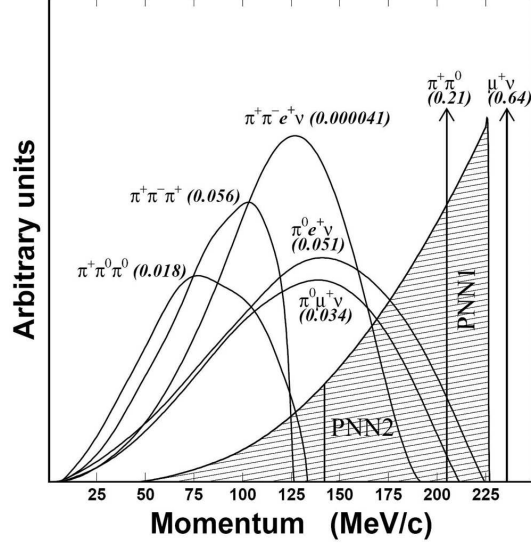


Fig. 3 Momentum spectra of charged particles from K^+ decay in the rest frame. The values in the parentheses represent the branching ratios for their decay modes. The hatched spectrum shows pion momentum in $K^+ \rightarrow \pi^+ \nu \bar{\nu}$ decay assuming $V-A$ interaction.

sensitive to $K^+ \rightarrow \pi^+ \nu \bar{\nu}$ decay than $\pi \nu \bar{\nu}(2)$ due to less number of background's sources.

3.1 Analysis strategy

Since the predicted branching ratio for $K^+ \rightarrow \pi^+ \nu \bar{\nu}$ in the SM is at 10^{-10} , the backgrounds should be suppressed to the level of 10^{-11} . This large suppression of the backgrounds makes a reliable estimation of the backgrounds in the signal region difficult, because any measurement involving low statistics could be subject to large statistical fluctuations. To find the candidate events we used a "blind" analysis. That is, background sources are identified a priori and a signal region is masked out until the selection criteria (cuts) development and the background estimation are finalized. For a background study the real data are divided into two portions: a uniformly-sampled one-third portion of the whole data is used to develop the cuts, and the remaining two-third portion is used to measure the final background levels.

The bifurcation method is used for the background estimation. The estimation is performed with two uncorrelated cuts or groups of cuts, which are independently inverted to enhance of statistics. This method is shown in Figure 4. The number of

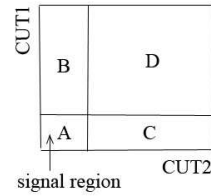


Fig. 4 Schematic of bifurcation method. The background level in signal region can be estimated from the numbers of events observed in the other regions.

background events in the signal region is A events. If the two cuts are uncorrelated, that is, if the rejection of a cut does not depend on the rejection of the other cut, the ratio of the number of background events in region "A" to region "B" must be equal to the ratio in region "C" to region "D". Therefore number of background events in the signal region is $A = BC/D$.

4 Backgrounds: suppression and estimation

4.1 Overview

Figure 5 shows the range in a plastic scintillator versus the momentum of charged

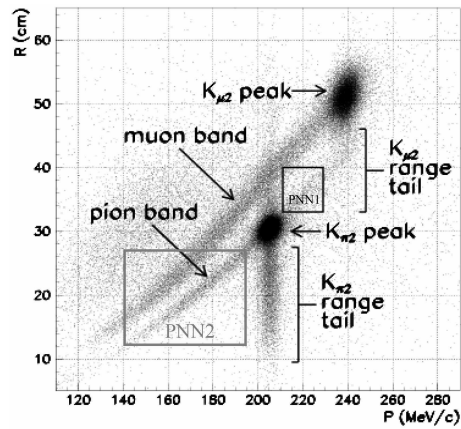


Fig. 5 Range in a plastic scintillator and the momentum of the charged particles for events that pass the $K_{\pi 2}$ trigger.

particles for the events that pass the $K_{\pi 2}$ trigger [3]. There are various sources of background in this figure. Events in the $K_{\pi 2}$ peak due to π^+ track from $K^+ \rightarrow \pi^+ \pi^0$ decays with a momentum of 205 MeV/c, an energy of 108 MeV and a range of 30 cm. Events in the $K_{\mu 2}$ peak due to μ^+ track from $K^+ \rightarrow \mu^+ \nu_{\mu}$ decays with a momentum of 236 MeV/c, an energy of 153 MeV and a range of 55 cm. Both events in the $K_{\pi 2}$ range tail and events in the $K_{\mu 2}$ range tail have ranges smaller than that expected from these decays, due to elastic (inelastic) scattering in the RS. Events in the muon band are due to multibody decays, such as $K^+ \rightarrow \mu^+ \nu_{\mu} \gamma$ (radiative $K_{\mu 2}$ or $K_{\mu \nu \gamma}$) and $K^+ \rightarrow \mu^+ \pi^0 \nu_{\mu}$ ($K_{\mu 3}$), π^+ decay in flight in the target and the $K_{\mu 2}$ decay with inelastic scattering in the target. Events in the pion band are due to pions in the beam that scatter into the RS.

4.2 $K_{\pi 2(\gamma)}$ background

The $K_{\pi 2(\gamma)}$ background consists of three components: $K_{\pi 2}$ -target scatter, $K_{\pi 2}$ -range stack scatter and $K^+ \rightarrow \pi^+ \pi^0 \gamma$ decay ($K_{\pi 2\gamma}$). If photons from π^0 decay were missed and π^+ lose energy due to scattering, then $K_{\pi 2}$ event appears in the signal region. The positive pion from $K_{\pi 2\gamma}$ decay is not monochromatic, therefore three final-state photons should be miss for this type of event to be a background.

The main background for this analysis is $K_{\pi 2}$ decay in which the π^+ travels along the kaon fiber, loses energy and scatters in the target, while π^0 travels parallel to beam direction and photons from its decay are directed at upstream or downstream ends of the detector where the photon veto is weakest. Two cuts used for suppression of this background were photon veto and target-scatter cuts. Pion scattering was identified by kinks in the pattern of target fibers attributed to pion, by tracks that didn't point back to the fiber containing the kaon decay, by energy deposits inconsistent with an outgoing pion or by unexpected energy deposits at the time of the pion in fibers traversed by the kaon. There is also a much smaller background due to $K_{\pi 2}$ -range stack scattering that is similarly identified by the energy deposits and pattern of RS counters attributed to the track.

$K_{\pi 2\gamma}$ background could not be distinguished from the larger $K_{\pi 2}$ -scatter background based solely on the π^+ track. The rejection of this background was calculated using a combination of simulated $K_{\pi 2}$ and $K_{\pi 2\gamma}$ events and $K_{\pi 2}$ data events.

4.3 $K^+ \rightarrow \pi^+ \pi^- e^+ \nu_e$ (K_{e4}) background

The branching ratio of the K_{e4} decay is $(4.09 \pm 0.10) \times 10^{-5}$ [11] and this process forms a background when the π^- and e^+ have little kinetic energy and interact in the target without leaving a detectable trace. Figure 6 shows the total kinetic energy of the π^- and e^+ versus the π^+ momentum for simulated events passed the trigger. For these low kinetic energy events the distribution of the π^+ momentum

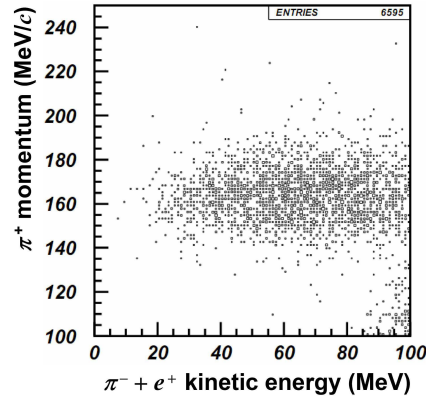


Fig. 6 Total kinetic energy of the π^- and e^+ versus the π^+ momentum for simulated events passed the trigger.

concentrates around 160 MeV/c which is in the range of the $\pi\nu\bar{\nu}(2)$ signal region ($140 \text{ MeV} < P_\pi < 199 \text{ MeV}$). Due to low statistics and contamination by the other types of background it was not possible to make a purely data-based background sample for bifurcation analysis. So both data and simulated data were used to estimate this background. Positron interaction are well-modeled in EGS4-based simulation and the π^- energy deposition spectrum in scintillator measured previously in E787 [5] was used to model π^- absorption. To isolate K_{e4} sample the target pattern recognition was used. The simulated data supplemented by the π^- energy deposition spectrum in scintillator were used to estimate the rejection power of the target pattern recognition.

4.4 Charge exchange background

Interaction of incoming kaon in the target $K^+n \rightarrow K^0p$ can be a source of background when the K^0 decays as K_S^0 or K_L^0 . The time condition requirement effectively removes any contribution from short-lived K_S^0 ($\tau_{life} = 0.1 \text{ ns}$). The semileptonic decays $K_L^0 \rightarrow \pi^+e^-\bar{\nu}_e$ and $K_L^0 \rightarrow \pi^+\mu^-\bar{\nu}_\mu$ with branching ratio of 20% and 14%, respectively, are the most likely sources of background of this type. The charge exchange event has a gap between kaon and pion fibers in the target. It is therefore suppressed by requiring no large gap between kaon and pion fibers. To identify these gaps the target pattern recognition was used. This background is also suppressed by the time condition requirement since K_L^0 that travels a short distance can be allowed by requiring no large gap. Additional suppression is provided by detecting the negative lepton. It is not possible to isolate a sufficiently pure, statistically significant sample of charge exchange events so the rejection power of the cuts was measured with simulated data.

4.5 Muon background

$\pi\nu\bar{\nu}(2)$ signal region extends from 140 to 199 MeV in π^+ momentum, therefore $K^+ \rightarrow \mu^+ \nu_\mu$ decay with monochromatic muon momentum of 236 MeV cannot be a background. Due to this kinematic constrain only multibody decays $K^+ \rightarrow \mu^+ \pi^0 \nu_\mu$ and $K^+ \rightarrow \mu^+ \nu_\mu \gamma$ are important. These decays require muon to be misidentified as a pion in order to be a background. Muons and pions have the different kinematic parameters (as shown in Figure 5), therefore one of two bifurcation cuts for suppression muon background is the π/μ range-momentum separation and another one is $\pi \rightarrow \mu \rightarrow e$ decay chain identification. This decay chain identification relies almost entirely on the analysis of the transient digitizer data (TD cut). In this analysis TD cut was loosened compared to $\pi\nu\bar{\nu}(1)$ analysis [3] to increase the acceptance since the muon background is very small and continues to be much smaller than other background after loosening.

4.6 Beam background

The non- K^+ decay background contains three component: charge exchange interaction (Section 4.4), Single Beam and Double Beam backgrounds.

The Single Beam background can be further categorized into two types: kaon entering and pion entering cases. If a single kaon entering the apparatus decays in flight to π^+ , the kinematic values of the positive pion can shift up to higher due to a Lorentz boost. If two photons are missed, such an event can fake the $K^+ \rightarrow \pi^+ \nu\bar{\nu}$ signal. The kaon decay-in-flight events tend to have earlier decay timings in the target than the stopped kaon decay event. The Single Kaon Beam background is suppressed by imposing a delayed coincidence (DC) to the decay time. If a pion in the beam scatters in the target and then enters the fiducial region of the detector, the event fakes the $K^+ \rightarrow \pi^+ \nu\bar{\nu}$ signal. The scattered pion leaves the target immediately after entering the target. This type of Single Beam background is also suppressed by the DC. It is also suppressed by kaon identification in the Čerenkov counter and the beam hodoscope.

The Double Beam background can also be categorized into two: kaon-kaon entering and kaon-pion entering cases. In the kaon-kaon entering case the first kaon enters and stops the target, and the second kaon entering the target decays-in-flight to π^+ and the π^+ enters the fiducial region of the detector. The kaon-pion case is the same as the kaon-kaon case, except that the second pion scatters in the target and enters the fiducial region to satisfy the kinematics of the signal. For both cases the Double Beam background can imitate $K^+ \rightarrow \pi^+ \nu\bar{\nu}$ signal, if the decay products from the first kaon are missed and the second kaon or pion is not detected in the beam line detectors. These backgrounds can be suppressed by looking for any extra activities that are coincident with the charged track in the beam instrumentation, target and range stack.

4.7 Background summary

The contribution of the each background component and the total background are presented in Table 2. Compared to E787 $\pi \nu \bar{\nu}(2)$ analysis [2], our total background

Table 2 Summary of the estimated number of events in the signal region from each background component for E787 and E949 $\pi \nu \bar{\nu}(2)$ analysis. In the third column the first value is the sum of $K_{\pi 2}$ -target scatter and $K_{\pi 2}$ -range stack scatter events.

Process	Background events (E949)	Background events (E787)
$K_{\pi 2}$ -target scatter	$0.619 \pm 0.150^{+0.067}_{-0.100}$	1.030 ± 0.230
$K_{\pi 2}$ -range stack scatter	$0.030 \pm 0.005 \pm 0.004$	
$K_{\pi 2\gamma}$	$0.076 \pm 0.007 \pm 0.006$	0.033 ± 0.004
K_{e4}	$0.176 \pm 0.072^{+0.233}_{-0.124}$	0.052 ± 0.041
Charge exchange	$0.013 \pm 0.013^{+0.010}_{-0.003}$	0.024 ± 0.017
Muon	0.011 ± 0.011	0.016 ± 0.011
Beam	0.001 ± 0.001	0.066 ± 0.045
Total	$0.927 \pm 0.168^{+0.320}_{-0.237}$	1.22 ± 0.24

was decreased by 24% and total acceptance was increased by 63% thanks to improved background rejection due to the upgrades of the AD and BV for E949. In addition the improved knowledge of the background contributions allowed the signal region to be divided into nine sub-regions, with relative signal-to-background levels differing by a factor of 4, that were used in the likelihood method [10] to determine $BR(K^+ \rightarrow \pi^+ \nu \bar{\nu})$.

5 Results

After completion of the background studies, the signal region was examined and three candidates were found. The energy versus range for these observed candidates is shown in Figure 7 along with the results of previous E787 [1, 2] and E949 [3, 4] analyses. From these three new candidates alone, $BR(K^+ \rightarrow \pi^+ \nu \bar{\nu}) = (7.89^{+9.26}_{-5.10}) \times 10^{-10}$ was calculated using the likelihood method [10]. The probability of these three events to be due to background only is 3.7%. When combined with the results of previous E787 and E949 analyses, $BR(K^+ \rightarrow \pi^+ \nu \bar{\nu}) = (1.73^{+1.15}_{-1.05}) \times 10^{-10}$ was measured. The probability that seven candidate events were due to background only is 0.1%. These observation imply a $K^+ \rightarrow \pi^+ \nu \bar{\nu}$ branching ratio consistent with SM prediction.

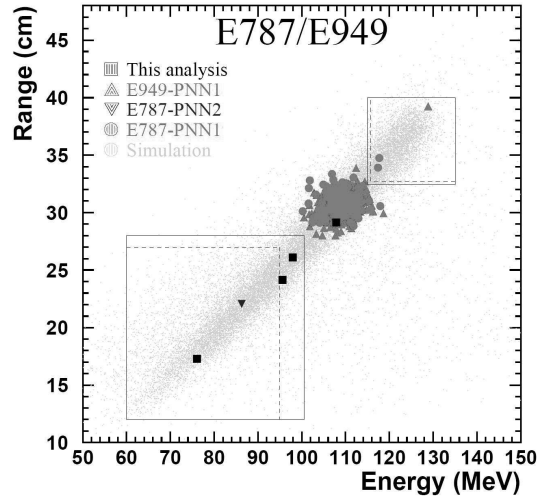


Fig. 7 The kinetic energy vs. range of all candidate events passing all other cuts. The points near $E_\pi = 108$ MeV are $K_{\pi 2}$ that survive the photon veto cuts and predominantly from the $\pi\nu\bar{\nu}(1)$ analyses due to the higher sensitivity and the less stringent photon veto cuts. No kinematic cuts are applied to the simulated $K^+ \rightarrow \pi^+\nu\bar{\nu}$ events (light grey).

6 Conclusion

For many years physics beyond the Standard Model, or new physics, has been searched for. There are two approaches: one is the direct search of new particles in a very high-energy region; the other is the observation of any possible discrepancy between measured and predicted quantities in electroweak processes. The search for the decay $K^+ \rightarrow \pi^+\nu\bar{\nu}$ is an attempt to utilize the latter of two approaches.

In 25 years of research with BNL E787 and E949, the search for $K^+ \rightarrow \pi^+\nu\bar{\nu}$ decays went from a limit on the branching ratio $BR(K^+ \rightarrow \pi^+\nu\bar{\nu}) < 1.4 \times 10^{-7}$ at 90% CL to a measurement of $(1.73^{+1.15}_{-1.05}) \times 10^{-10}$ that is twice as large as, but still consistent with, the Standard Model expectation of $(0.85 \pm 0.07) \times 10^{-10}$.

There is a letter of intent for a stopped kaon decay experiment in Japan. And analysis of E949/E787 for other K^+ decay modes still continue.

Experiment NA62 (formerly NA48/3) at CERN was approved in 2007 and is in preparation. The use of kaon decay-in-flight to measure $K^+ \rightarrow \pi^+\nu\bar{\nu}$ has not been attempted before. NA62 proposes to observe about 65 $K^+ \rightarrow \pi^+\nu\bar{\nu}$ events using 75 GeV/c beam.

References

1. S. Adler et al., Phys. Lett. B. **537**, 211 (2002)
2. S. Adler et al., Phys. Rev. D. **70**, 037102 (2004)
3. S. Adler et al., Phys. Rev. D. **77**, 052003 (2008)
4. V.V. Anisimovky et al., Phys. Rev. Lett. **93**, 031801 (2004)
5. M. Ardebili, Ph.D. Thesis, *Princeton University* (1995)
6. Y. Asano et al., Phys. Lett. B. **107**, 159 (1981)

7. J. Brod, M. Gorbahn, Phys. Rev. D. **78**, 034006 (2008)
8. A.J. Buras, Nucl. Phys. B **697**, 2004
9. U. Camerini, D. Ljung, M. Sheaff, D. Cline, Phys. Rev. Lett. **23**, 326 (1969)
10. T. Junk, Nucl. Instrum. Meth. A. **434**, 435 (1999)
11. W.M. Yao et al., J. Phys. G **33**, 1 (2006)